Mono- and Bi-specific Nanobodies Targeting the CUB Domains of PCPE-1 Reduce the Proteolytic Processing of Fibrillar Procollagens

Priscillia Lagoutte, Jean-Marie Bourhis, Natacha Mariano, Virginie Gueguen-Chaignon, David Vandroux, Catherine Moali, Sandrine Vadon-Le Goff

Research Article

Mono- and Bi-specific Nanobodies Targeting the CUB Domains of PCPE-1 Reduce the Proteolytic Processing of Fibrillar Procollagens

Priscillia Lagoutte [1], Jean-Marie Bourhis [2], Natacha Mariano [1], Virginie Gueguen-Chaignon [3], David Vandroux [4], Catherine Moali [1] and Sandrine Vadon-Le Goff [1,*]

*1 - **Universite Claude Bernard Lyon 1,** CNRS, Tissue Biology and Therapeutic Engineering Laboratory, LBTI, UMR5305, F-69367 Lyon, France*

*2 - **Institut de Biologie Structurale,** University Grenoble Alpes, CEA, CNRS, F-38000 Grenoble, France*

*3 - **Protein Science Facility,** SFR BioSciences, Univ Lyon, CNRS UAR3444, Inserm US8, ENS de Lyon, F-69367 Lyon, France*

*4 - **NVH Medicinal,** F-21000 Dijon, France*

***Correspondence to Sandrine Vadon-Le Goff:** sandrine.legoff@ibcp.fr (S. Vadon-Le Goff)*

https://doi.org/10.1016/j.jmb.2024.168667

Edited by S. Koide

Abstract

The excessive deposition of fibrillar collagens is a hallmark of fibrosis. Collagen fibril formation requires proteolytic maturations by Procollagen N- and C-proteinases (PNPs and PCPs) to remove the N- and C-propeptides which maintain procollagens in the soluble form. Procollagen C-Proteinase Enhancer-1 (PCPE-1, a glycoprotein composed of two CUB domains and one NTR domain) is a regulatory protein that activates the C-terminal processing of procollagens by the main PCPs. It is often up-regulated in fibrotic diseases and represents a promising target for the development of novel anti-fibrotic strategies. Here, our objective was to develop the first antagonists of PCPE-1, based on the nanobody scaffold. Using both an *in vivo* selection through the immunization of a llama and an *in vitro* selection with a synthetic library, we generated 18 nanobodies directed against the CUB domains of PCPE1, which carry its enhancing activity. Among them, I5 from the immune library and H4 from the synthetic library have a high affinity for PCPE-1 and inhibit its interaction with procollagens. The crystal structure of the complex formed by PCPE-1, H4 and I5 showed that they have distinct epitopes and enabled the design of a biparatopic fusion, the diabody diab-D1. Diab-D1 has a sub-nanomolar affinity for PCPE-1 and is a potent antagonist of its activity, preventing the stimulation of procollagen cleavage *in vitro.* Moreover, Diab-D1 is also effective in reducing the proteolytic maturation of procollagen I in cultures of human dermal fibroblasts and hence holds great promise as a tool to modulate collagen deposition in fibrotic conditions.

Introduction

Fibrillar collagens are the most abundant proteins in the human body and the main components of a great variety of extracellular matrix networks. They shape organs and tissues and play crucial roles in maintaining their homeostasis or in promoting their correct repair after injury. Fibrillar collagens are synthesized as soluble precursor molecules, the procollagens, and proper assembly of collagen fibrils requires the proteolytic release of the N- and C-terminal propeptides found in procollagens. The BTPs (bone morphogenetic protein-1 (BMP-1)/tolloid-like proteinases) are the main proteases responsible for the removal of the C-propeptides of fibrillar procollagens, which is generally

considered as the rate-limiting step in collagen fibril formation.[1–3]

Excessive deposition of fibrillar collagens is a major feature of fibrosis. Fibrotic diseases largely contribute to morbidity and mortality worldwide.[4] They can target any organ and arise from a very broad range of pathological conditions such as myocardial infarction, chronic kidney disease, non-alcoholic steatohepatitis (NASH), scleroderma, corneal scarring or infections.[5,6] A recent example is the COVID-19 pandemic with infected patients presenting fibrotic damages in multiple tissues (lung but also kidney, heart etc.).[7] With an annual combined incidence of fibrotic diseases estimated to be around 5 per 100 person-years[8] and very few efficient therapeutic options,[5,6,9] there is a critical need for new anti-fibrotic drugs.

The main pathogenic factor in fibrosis is the abnormal accumulation of extracellular matrix, principally made of fibrillar collagens I and III.[9] Blocking the proteolytic maturation of these collagens should dramatically reduce their integration in the insoluble extracellular matrix and is thought to represent a relevant strategy to develop new anti-fibrotic therapies. BTPs are prime targets but, besides procollagens, they process many other substrates involved in various collagen-unrelated pathways (e.g. growth factor activation, angiogenesis, mineralization, lipid metabolism, peripheral nervous system development),[10] meaning that inhibiting their activity could lead to unwanted side effects.

Another key regulator of collagen fibrillogenesis is PCPE-1 (Procollagen C-Proteinase Enhancer-1), a secreted glycoprotein that specifically stimulates the C-terminal processing of fibrillar procollagens by BTPs.[11,12] PCPE-1 is composed of two CUB (Complement-Uegf-BMP-1) domains and of one C-terminal NTR (Netrin-like) domain, separated by a long linker (44 residues in human PCPE-1). The CUB domains are necessary and sufficient for PCPE-1 activity and this is due to their unique ability to bind the C-propeptides of collagens I-III with high affinities.[13,14] This interaction is thought to allow local unraveling of the procollagen trimer which facilitates the cleavage by the BTPs,[15,16] and explains why PCPE-1 has no effect on other BMP-1 substrates. The RNA and protein levels of PCPE-1 are increased in most fibrotic diseases and this protein appears as a promising target to monitor or treat fibrosis.[17] However, to date, no drug capable of blocking the interaction between PCPE-1 and procollagen C-propeptides has been reported.

In the past few years, simple immunoglobulin scaffolds, devoid of the undesired properties of conventional immunoglobulins (large molecular weight, hetero-tetrameric composition, disulfide bonds), have emerged as alternatives to classical antibodies. Among them, nanobodies, also called VHHs (Variable Heavy-chain domains of Heavy-chain only antibodies), derived from the heavy chain of camelid immunoglobulins, have been discovered in the early 90s.[18] Nanobodies are the smallest antibody fragments (around 15 kDa). They are highly soluble and stable and can be easily produced in high quantity in prokaryotic systems. Moreover, their convex paratope is well suited to bind difficult-to-target cavities at the surface of antigens. Three types of libraries can be used to select antigen-specific nanobodies: naive, immune or synthetic libraries.[19] Immune libraries are generated through the immunization of a camelid with the target, and usually give results more efficiently than naïve libraries.[19] Immune libraries are thus the most widely used nanobody libraries, yet some targets are not immunogenic or too toxic for animal immunization. Due to these limitations, several synthetic libraries have been developed.[20,21] In all cases, a bio-panning selection is carried out to retrieve specific VHHs from the library. To date, more than 1400 VHHs have been successfully selected (https://sda-db.ca).[22] Their very favorable characteristics have turned them into perfect tools for a wide range of applications including research, diagnostics and therapeutics.[19,23–27] In this field, caplacizumab, a nanobody used to treat acquired thrombotic thrombocytopenic purpura patients, and ozoralizumab, an anti-TNF-α developed for the treatment of rheumatoid arthritis, are the first approved nanobody-based drugs.[28,29] The use of nanobodies to diagnose or treat COVID-19 has also been heavily explored in recent years.[30,31] Nanobodies can also be engineered to fulfill both diagnostic and therapeutic roles, as recently exemplified with the development of VHHs targeting the immune modulator SIRPα protein.[32]

In this study, we generated nanobodies against the CUB1 and CUB2 domains of PCPE-1. We identified two nanobodies which behaved as tight binders of PCPE-1 with distinct binding sites, as revealed by surface plasmon resonance (SPR) and X-ray crystallography. Their association into a bispecific nanobody gave rise to a powerful antagonist of PCPE-1, which efficiently reduces procollagen maturation. This molecule could serve as a template for the development of diagnostic or therapeutic tools in the context of fibrotic diseases.

Results

Selection and characterization of nanobodies directed against PCPE-1

Since the CUB1 and CUB2 domains of PCPE-1 are necessary and sufficient for its PCP enhancing activity,[13] we used a truncated protein (CUB1CUB2), containing these two domains but lacking the NTR domain, as the antigen for the selection of nanobodies. In order to avoid non-specific binders, the tags added for the efficient purification of the protein were removed prior to selection. Two different strategies were carried out

(Figure 1a): an *in vivo* selection based on the immunization of a llama and an *in vitro* selection using a synthetic library of VHHs.[20]

For the immune library generation, nanobodies were raised through five successive injections of recombinant CUB1CUB2 followed by two rounds

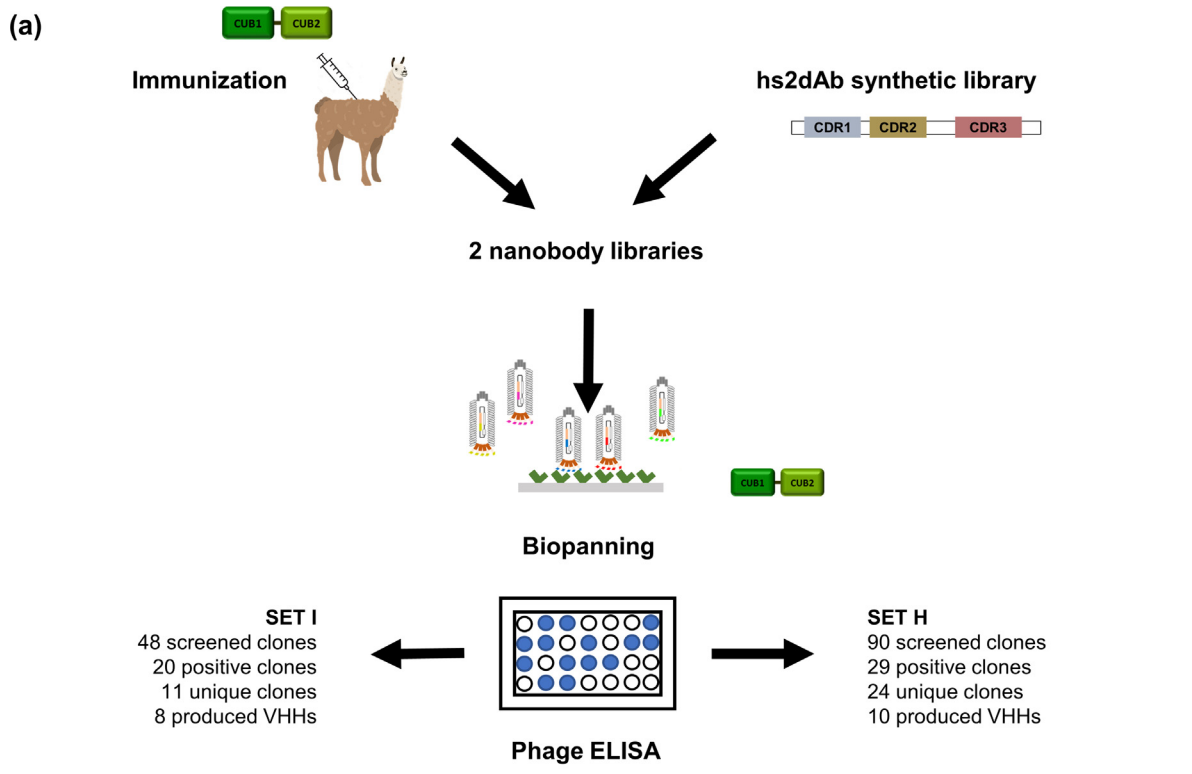

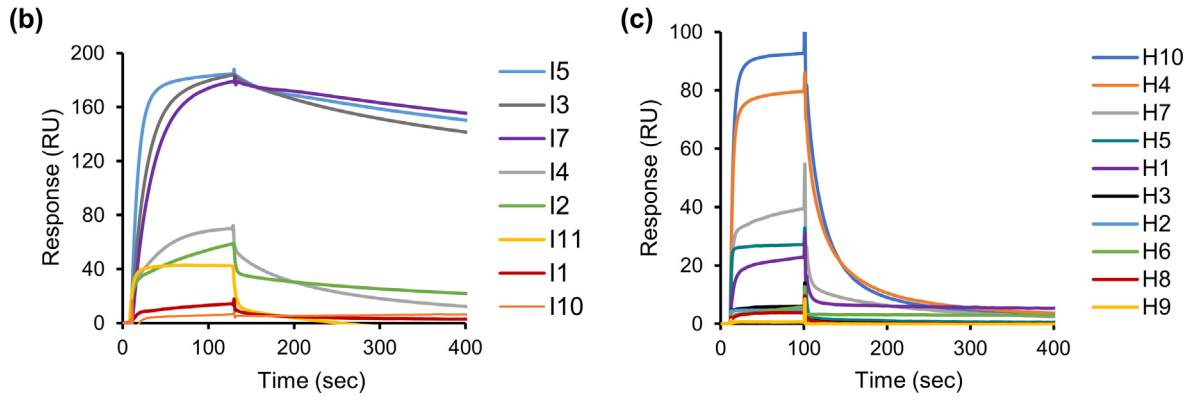

Figure 1. Overview of the generation and selection of nanobodies directed against CUB1CUB2 and preliminary characterization of their binding to full-length PCPE-1. (a) Two different libraries of nanobodies, one generated through the immunization of a llama (set I) and one synthetic library (set H), were used to select binders directed against the CUB1CUB2 domains of PCPE-1. Two and three rounds of phage display biopanning respectively allowed enrichment in specific nanobodies that were isolated by phage ELISA. Positive clones were sequenced, expressed and purified for further characterization. (b, c) Binding of the selected nanobodies to full-length PCPE-1 analyzed by SPR: 200 nM (b, set I – immune library) or 250 nM (c, set H – synthetic library) of each VHH were injected over immobilized PCPE-1 (b: 785 RU, c: 430 RU).

of bio-panning (Figure 1a). 48 clones were screened by phage ELISA corresponding to 11 unique clones after sequencing (set "I"). Among those, six families of VHHs could be distinguished based on their CDR3 sequences (Figure S1a). The first family was the most represented with five clones whereas other families had only one or two variants. Three members of family one (VHH-I1, VHH-I5 and VHH-I7) and one member of each of the other families (VHH-I2, VHH-I3, VHH-I4, VHH-I10 and VHH-I11) were selected, produced in the periplasm of *E. coli* and purified to homogeneity (Figure S2a). All were obtained as monomers after size exclusion chromatography. Their affinity for full-length PCPE-1 was measured by SPR (Figures 1b and S3). All VHHs except VHH-I10 were able to interact with PCPE-1 (Figure S3). VHH-I3, -I5, -I7 acted as strong binders of PCPE-1, with dissociation constants in the low nanomolar range and slow off-rates which could be calculated using a 1:1 binding model (Table 1 and Figure S3c, e, f). The other four nanobodies had lower affinities and the corresponding binding curves did not give satisfactory results with the 1:1 binding model. In this case, the heterogenous ligand model and steady-state analysis, using the binding response at the end of injection, were both used to estimate their K_Ds (Table 1). Interestingly, the VHHs belonging to family one display very different binding behaviors: the interaction of VHH-I1 with PCPE-1 is weak with a fast dissociation (Figure S3a), whereas VHH-I5 and -7 are the strongest binders, with K_Ds around 2 nM and slow dissociation rates (Figure S3e, f). To determine which domain of PCPE-1 was recognized by the best binders, competition experiments were performed using isolated CUB1 or CUB2 domains (Figures 2a and S4). When co-injected with CUB2, VHH-I3, -I5 and -I7 were unable to bind to immobilized PCPE-1, whereas in the same condition co-injection with CUB1 had almost no effect, showing that these nanobodies were mainly interacting with the CUB2 domain of PCPE-1. VHH-I11 was an exception, with partial inhibition of its binding by both CUB1 and CUB2.

Selection of binders from the synthetic library (set "H") was performed using three rounds of phage display; 90 VHH clones were picked and tested by phage ELISA for their binding to CUB1CUB2. 32% of the clones were positive and their sequencing revealed the presence of 24 unique VHHs. To favor the selection of nanobodies targeting the CUB1 domain of PCPE-1, we added a second round of phage ELISA, this time against the immobilized CUB1NTR region of PCPE-1. Ten VHHs, including 7 positive clones for CUB1NTR binding, were finally chosen for production (Figures S1 and S2b) and their affinity for full-length PCPE-1 was also measured by SPR (Figures 1c and S3). Only half of the selected clones showed substantial binding to PCPE-1 at 250 nM, the best results being obtained for VHH-H4 and VHH-H10 which had K_Ds in the low nanomolar range (Table 1, Figure S3h and i, best fits obtained with the heterogenous ligand model, $K_{D1} \approx 20$ nM, $K_{D2} \approx 2$ nM). The interaction of PCPE-1 with both VHHs-H4 and -H10 was inhibited by the co-injection of CUB1, but not of CUB2, confirming that these nanobodies mainly interacted with the CUB1 domain (Figures 2a and S4e, f).

For the best binder of each set (I5 and H4), we then tested whether they were able to bind to PCPE-1 simultaneously. For this purpose, VHHs were injected on a PCPE-1 surface already saturated with VHH-I5 or -H4. While no changes were observed when VHH-I5 was co-injected with the other immune-derived nanobodies (with the exception of VHH-I11, see below), the simultaneous injection of VHH-I5 and synthetic VHH-H4 or -H10 resulted in an increased signal (Figures 2b and S5a), indicating that they bound to non-overlapping sites in PCPE-1. Similarly, when the surface was first saturated with VHH-H4 (Figures 2c and S5b), the immune-derived VHHs were still able to bind efficiently whereas VHH-H10 could not bind. These results confirm that the two sets of binders have non-overlapping epitopes but that within each nanobody set, the epitopes are mostly conserved, or close enough to prevent simultaneous binding due to steric clashes. The exception was VHH-I11 that was able to bind, although weakly, together with both VHH-I5 and VHH-H4, suggesting that it recognized a third and less represented epitope in PCPE-1, probably located in between CUB1 and CUB2 (Figure 2a).

PCPE-2 is another procollagen C-proteinase enhancer, sharing 43% sequence identity with PCPE-1, which was recently reported to have both common functions with PCPE-1 and additional specific activities.[33] It was therefore necessary to check whether the PCPE-1-directed binders also bound to PCPE-2. For this purpose, VHH-I5 and VHH-H4 were site-specifically biotinylated on their C-terminus via sortase coupling and immobilized on a streptavidin chip. In both cases, the interaction with PCPE-2 was almost undetectable ($K_D > 1$ μM) while PCPE-1 bound very tightly ($K_D = 1.5$ nM and $K_D = 3.9$ nM with the 1:1 binding model for VHH-I5 and VHH-H4 respectively, Figure 2d, e). Therefore, the affinities of VHH-I5 and -H4 are more than 1000-fold higher for PCPE-1 than for PCPE-2. Notably, in this SPR configuration, the heterogeneity previously observed for the interaction of VHH-H4 with PCPE-1 was not present and the data could be nicely fitted with the 1:1 binding model (Table 1).

Anti-CUB1CUB2 nanobodies are potent antagonists of PCPE-1

Since PCPE-1 activity is known to be mediated by its interaction with procollagen C-propeptides (K_D in the low nanomolar range),[16] we then investigated

Table 1 Binding affinities of the selected VHHs for PCPE-1, measured by SPR.

		Kinetics									Steady-state
		k_{a1} (10^6 M^{-1}·s^{-1})	k_{d1} (10^{-3} s^{-1})	K_{D1} (nM)	R_{max1} (%)	k_{a2} (10^6 M^{-1}·s^{-1})	k_{d2} (10^{-3} s^{-1})	K_{D2} (nM)	R_{max2} (%)	Chi^2 (RU^2)	K_D (nM)
Set I immune library	**I1**					NA					**> 400**
	I2	1.63	216	**132**	64	0.08	0.9	**10.9**	36	0.4	**154**
	I3	0.69	2.8	**4.1**	100	–	–	–	–	1.7	
	I4	1.75	581	**333**	94	0.12	3.2	**26.6**	6	0.1	**> 200**
	I5	1.60	2.8	**1.8**	100	–	–	–	–	2.9	
	I7	0.59	0.85	**1.4**	100	–	–	–	–	2.5	
	I11	1.13	288	**255**	80	0.39	5.7	**14.6**	20	2.5	**170**
Set H synthetic library	**H4**	1.79	40.6	**22.7**	61	1.25	2.8	**2.2**	39	0.8	**15**
	H10	1.54	39.3	**25.5**	80	1.86	5.2	**2.8**	20	1.2	**18**

Kinetic (k_a, k_d) and equilibrium (K_D) constants were determined by fitting the experimental data with the 1:1, the heterogeneous ligand or the steady-state binding models. Sensorgrams and best fits are given in Figure S3. NA: not applicable.

whether the selected VHHs were able to block the binding of PCPE-1 to a human mini-procollagen III (Mini-III) which includes all procollagen III C-terminal domains (end of triple helix, C-telopeptide and C-propeptide).[12] Competition experiments were carried out by SPR, and showed that VHH-I3, -I5, -I7, -H4 and -H10 inhibited PCPE-1 binding to Mini-III to various extents whereas VHH-I1, -I2, -I4 and -I11 did not affect the interaction when used at 250 nM (Figures 3a and S6). VHH-H4 and VHH-I5 were the most efficient of each set, with around 75% and 50% inhibition respectively. Furthermore, their antagonist effects were additive since the co-injection of 250 nM of a mix of VHH-I5 and VHH-H4 with PCPE-1 nearly completely abolished its interaction with immobilized Mini-III. This inhibition was also concentration-dependent, giving dose–response curves with half-maximal inhibitory concentrations (IC_{50}) around 45 nM (VHH-H4), 24 nM (VHH-I5) and 19 nM (mix of VHH-I5 and VHH-H4) in the presence of 5 nM PCPE-1 (Figure S6) in the conditions of the experiment. However, it was not possible to completely inhibit the interaction with VHH-I5 alone (maximum inhibition around 70%). This residual binding was not present when VHH-H4 and VHH-I5 were combined.

Since the VHHs compete with procollagen for PCPE-1 binding, the next step was to check if they could also block PCPE-1 activity *in vitro*. For this, we used CPIII-Long, another model substrate derived from human procollagen III. As previously described,[15] it was cleaved when incubated with recombinant BMP-1 and this cleavage was efficiently stimulated by PCPE-1 (Figure 3b, 2.4-fold enhancement in the conditions of the assay). Addition of VHH-I1, VHH-I2, VHH-I4 or VHH-I11 had very little effect on PCPE-1 enhancing activity. On the contrary, addition of VHH-I3, VHH-I5, VHH-I7, VHH-H4 or VHH-H10 led to a 40–80% decrease in cleavage stimulation and a total loss of enhancement was observed when VHH-I5 and VHH-H4 were added together. Interestingly also, the activity of BMP-1 itself did not seem to be modified by the nanobodies despite the fact that it also contains three CUB domains. This was coherent with the fact that the nanobodies did not interact with BMP-1 (Figure S7).

Altogether, these data suggest that the selected binders behave as strong antagonists of PCPE-1, able to hinder the stimulation of procollagen C-terminal maturation by PCPE-1.

High-resolution structure of the CUB domains of PCPE-1 bound to nanobodies VHH-I5 and VHH-H4

The complex formed by VHH-H4 and VHH-I5 bound to CUB1CUB2 was isolated by size exclusion chromatography and its structure was solved at high resolution (2.2 Å, Table 2, Figure 4a, PDB accession no. **9EN2**). All protein chains were complete except that electronic density was missing for the inter-domain linker (residues 151–157, numbering starting with the first residue of the signal peptide) of CUB1CUB2. As predicted from the binding experiments, VHH-I5 was found to bind mainly to CUB2 whereas VHH-H4 bound to CUB1. More surprisingly, VHH-H4 also makes contacts with CUB2 and occupies the interface between the two CUB domains, thereby locking CUB1CUB2 in a closed configuration and preventing inter-domain flexibility (Figure 4). However, we cannot exclude the possibility that the observed structural arrangement is due to crystal packing and could potentially differ in solution.

For VHH-H4, the surface of the interface was calculated by the PISA webserver[34] to be 1000 $Å^2$. Most of the residues involved in the interaction with CUB1 belong to CDR3. Glu100 forms a hydrogen bond with Tyr47 (CUB1), while Leu108 is embedded in a hydrophobic cavity formed by Phe35, Tyr47, Phe53, Pro54 and Leu143 (Figure 4b). This interaction is further stabilized by a π-stacking between Trp107 (VHH-H4) and Arg32 (CUB1) (Figure 4b). Furthermore, Lys77, belonging to the framework of VHH-H4, makes multiple con-

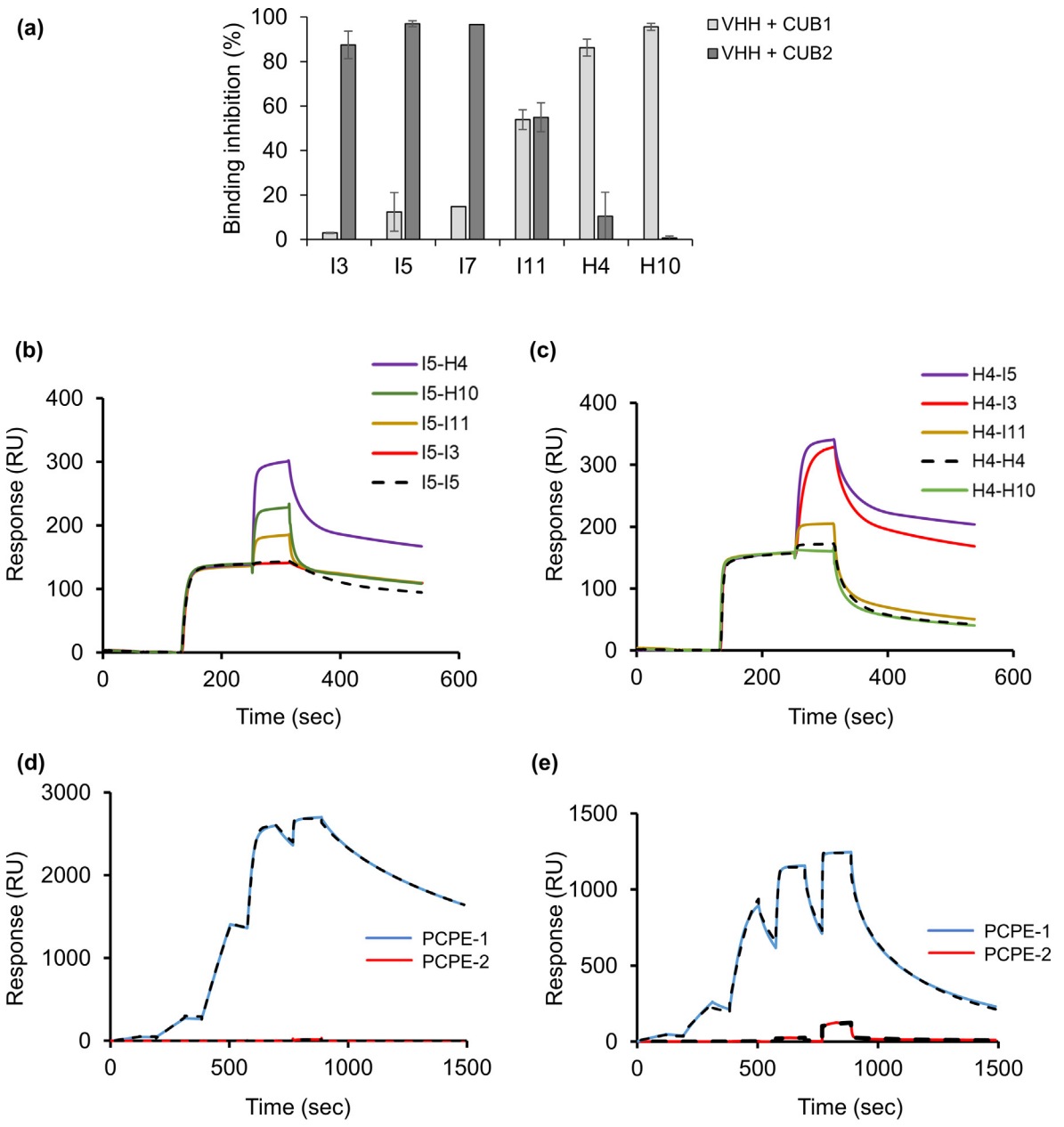

1:1 binding model		k_a (10^6 $M^{-1}{\cdot}s^{-1}$)	k_d (10^{-3} s^{-1})	K_D (nM)
I5	**PCPE-1**	0.94	1.4	**1.45**
	PCPE-2	-	-	**> 1000**
H4	**PCPE-1**	3.6	13.1	**3.85**
	PCPE-2	-	-	**> 1000**

Figure 2. Characterization of PCPE-1/VHHs interactions. (a) Inhibition of the binding of VHHs (50 nM) to immobilized PCPE-1 (645 RU) by the co-injection of 250 nM CUB1 or CUB2 domain (means ± ranges; $n = 2$). (b, c) Injection of 250 nM VHH-I5 (b) or VHH-H4 (c) for 120 sec followed by an injection of the same concentration of VHH-I5 or VHH-H4, alone or in combination with 250 nM of a second VHH for another 90 sec (representative of $n = 2$ experiments). (d, e) Comparison of PCPE-1 (blue line) and PCPE-2 (red line) binding to VHH-I5 (d, 813 RU) and VHH-H4 (e, 491 RU). Sequential injections of increasing concentrations (0.8, 4, 20, 100 and 500 nM) of the analyte were carried out over biotinylated VHH-I5 and VHH-H4 captured on immobilized streptavidin ($n = 1$). Fits (dotted lines) were obtained with the kinetic 1:1 binding model.

tacts with the acidic residues of the Ca^{2+} binding site of CUB2 (Figure 4c).

In contrast, VHH-I5 establishes significant contact specifically with the CUB2 domain, as illustrated in Figure 4a and d. The interface surface, calculated using PISA, measures 610 Å^2. A polar network, involving residues from CDR1 (Asn32) and CDR2 (Ser52 and Ser56), engages with Asp238. Additionally, CDR1 (Thr33) and CDR2 (Ser52) form polar contacts with the backbone of Val240 of CUB2. We can also notice the presence of a salt bridge between Asp61 (a conserved core residue of VHH-I5) and Arg231 from CUB2 (Figure S8).

Diabody generation and characterization

The results described above suggested that combining nanobodies I5 and H4 in a bivalent fusion could further improve their affinity for PCPE-1 through cooperative mechanisms. Based on the crystallographic data, we determined that the C-terminal region of VHH-H4 was close enough to the N-terminal region (60 Å) of VHH-I5 to be fused with a $(GS)_n$ flexible linker. The fusion diabody D1 (diab-D1) was produced in bacteria and purified (Figure S2c). It eluted in size exclusion chromatography at the expected size of the biparatopic construct (around 30 kDa).

Interaction of diab-D1 with PCPE-1 was assessed by SPR analysis, giving an apparent dissociation constant (1:1 binding model) of 0.32 nM, that is 5 and 45 times lower than its parent components I5 and H4 (Figure 5a). The benefit of the association was also demonstrated by a much slower dissociation rate (k_d = 5.10^{-4} s^{-1}) than for the individual VHHs (k_d in the 10^{-3} or 10^{-2} s^{-1} range), as also evidenced in Figure S9.

Competition experiments were carried out to determine whether diab-D1 also had a higher antagonist effect against PCPE-1 than its parent components (Figure 5b). In the conditions of the

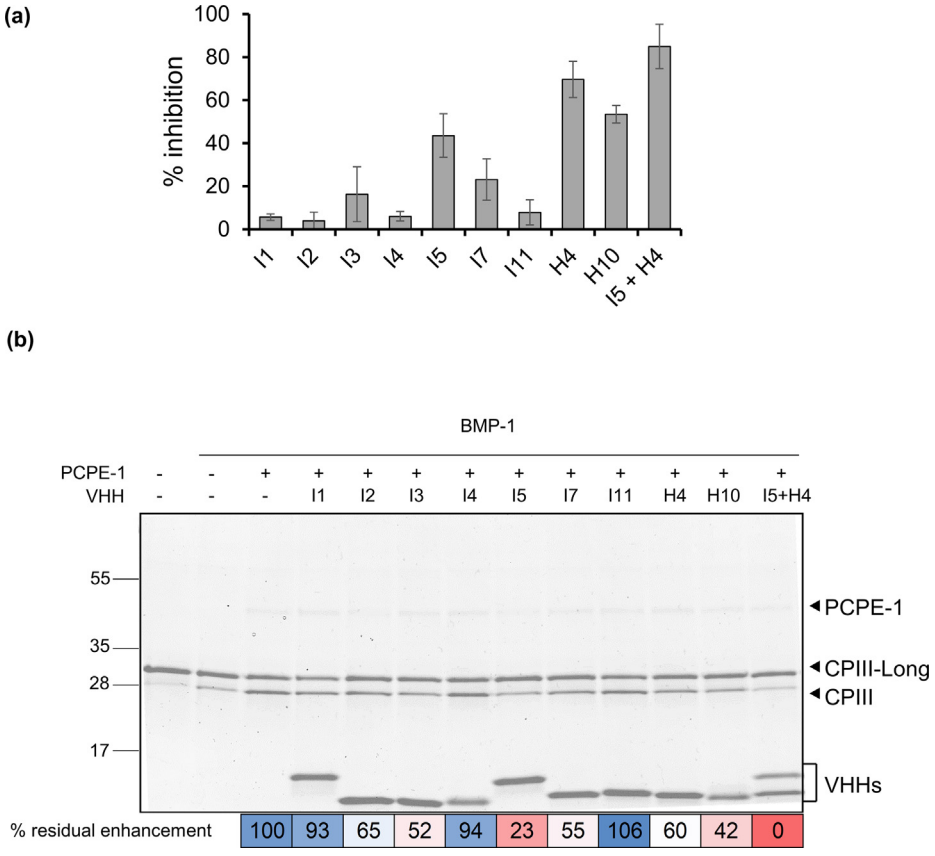

Figure 3. Inhibition of PCPE-1/procollagen interaction by the selected binders. (a) Competition experiments consisting of an injection of 5 nM PCPE-1 alone or in combination with 250 nM VHH(s) over immobilized Mini-III. Inhibition was measured by comparing the binding response (5 sec before the end of injection) obtained with PCPE-1 alone or in combination with the VHHs (means ± range; *n* = 2). (b) CPIII-Long was incubated with 3 nM BMP-1 and 75 nM PCPE-1 in the absence or presence of 2 μM (total concentration) VHH(s) for 1 h at 37 °C. Reaction products were analyzed by SDS-PAGE (4–20% polyacrylamide gel; reducing conditions) and Coomassie Blue staining. % residual enhancement by PCPE-1 (compared to BMP-1 alone condition) is shown below the gel (quantification by densitometry, color coding according to % value). The gel is representative of *n* = 3 independent experiments.

experiment (Figure 5b, same conditions as Figure S6), the IC_{50} value for diab-D1 inhibition of PCPE-1/Mini-III interaction was estimated to be 3.4 ± 0.2 nM, which is 5–15-fold lower than the IC_{50}s measured for VHH-I5 and VHH-H4 (alone or injected together). In line with the SPR data, addition of diab-D1 totally abolished the stimulation of CPIII-Long cleavage by PCPE-1 (Figure 5c). It was also able to prevent the enhancement of Mini-I or Mini-II cleavage by PCPE-1 (Figure S10a, b, Mini-I and Mini-II are short versions of human procollagens I and II).[33,35]

Diab-D1 was then evaluated in primary cell culture assays for its ability to modulate procollagen I processing (Figures 6 and S10c, d). The addition of 530 nM of diab-D1 in the culture medium of human dermal fibroblasts induced a marked reduction of procollagen I cleavage, with around 50% less C-propeptide released in the conditioned medium. This effect was maintained when exogenous PCPE-1 or TGFβ were added to mimic fibrotic conditions (Figure 6a, b). The same reduction in C-propeptide cleavage was seen when rat cardiac fibroblasts were used (Figure S10c, d).

Altogether, these results show that diab-D1 is a powerful antagonist of PCPE-1, capable of decreasing procollagen processing by primary cells.

Discussion

Given the central role played by fibrillar procollagens in the pathogenesis of fibrotic diseases, the proteins involved in their biosynthesis represent possible therapeutic targets.[5,8,9,36] Among them, PCPE-1 has recently emerged as a feature of fibrosis and as a potential biomarker.[17,37] It was also shown that PCPE-1 deficiency protected mice against liver fibrosis development and collagen deposition in a model of non-alcoholic steatohepatitis (NASH), demonstrating for the first time that PCPE-1 was instrumental for fibrosis development.[38] However, there is currently no demonstration that pharmacological targeting of PCPE-1 could be equally efficient, and the lack of available tools to modulate its activity was preventing a deeper characterization of PCPE-1 involvement in fibrotic pathologies. Here, we have developed the first antagonists able to block the interaction between PCPE-1 and procollagen C-propeptides, and to hinder PCPE-1 enhancing activity.

To target the interface between PCPE-1 and procollagen C-propeptides, we have chosen to generate nanobodies against the PCPE-1 domains directly involved in the interaction (CUB1CUB2). Through the immunization of a llama, we selected and characterized 8 nanobodies. Three of them exhibit nanomolar affinity for PCPE-1 and all happen to bind to its CUB2 domain. The CUB domains of PCPE-1 are highly conserved in mammals, and human and alpaca (*vigugna pacos*) CUB domains share 92% identity, with differences equally distributed between CUB1 and CUB2. It was therefore surprising to get only CUB2 ligands. To increase the diversity of the binders and our chance to select a strong antagonist of PCPE-1, we ran a second selection, this time using a synthetic library. The use of this *in vitro* method enabled us to drive the selection towards nanobodies targeting CUB1. As it is often the case with synthetic libraries,[19,39] these nanobodies have a lower affinity for PCPE-1 than the immune-derived ones, which were optimized through the adaptive immune system of the animal. Only two VHHs (VHH-H4 and VHH-H10) were found to bind efficiently to PCPE-1, but both were confirmed to interact with CUB1. Since VHH-H10 was more difficult to produce in high quantities, VHH-H4 was selected as the "CUB1 binder" prototype. It exhibits a very good capacity to inhibit PCPE-1 binding to procollagen, as does VHH-I5 from the immune library. Moreover, both can bind simultaneously to PCPE-1 and their antagonistic effects are additive.

All attempts to crystallize CUB1CUB2 in complex with only one VHH failed, probably because of the flexibility conferred by the linker between CUB1 and CUB2. In contrast, we obtained the high-resolution structure of the three-partner complex formed by CUB1CUB2, VHH-I5 and VHH-H4. It confirms that the two VHH bind to different epitopes, each located on one CUB domain. More surprisingly, whereas VHH-H4 alone is not able to bind to CUB2, the crystal structure shows that, in

Table 2 Data collection and refinement statistics.

Parameter	CUB1CUB2 – VHH-H4 – VHH-I5
Resolution (Å)	48.0–2.2
Space group	$P2_12_12_1$
Unit cell	
a, b, c (Å)	54.8, 95.9, 110.8
α, β, γ (°)	90, 90, 90
Total reflections	505,918
Unique reflections[a]	37,547
Rmerge	0.086
Multiplicity	4.8
Completeness (%)	99.2
$I/\sigma(I)$	1.68 (at 2.2 Å)
Rwork	0.21
Rfree	0.24
RMSD (bond lengths) (Å)	0.014
RMSD (angles) (°)	1.96
Ramachandran favored (%)	99.6
Ramachandran allowed (%)	0
Ramachandran outliers (%)	0.4
Average B factor ($Å^2$)	44
PDB ID	9EN2

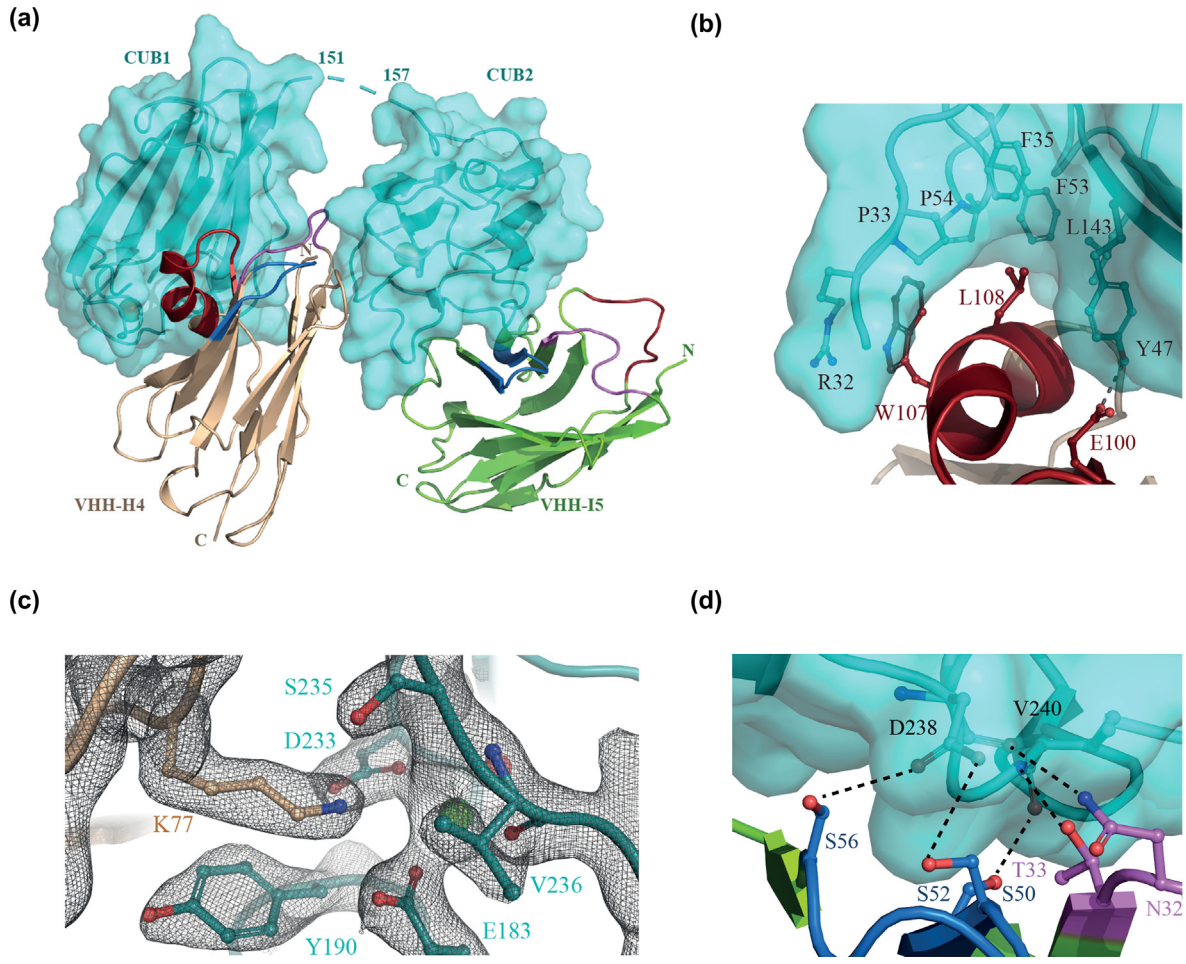

Figure 4. Crystal structure of the CUB domains of PCPE-1 in complex with VHH-H4 and VHH-I5 (PDB id 9EN2). (a) CUB1CUB2 is shown as a semi-transparent surface overlaying a cartoon representation colored in cyan. The calcium ions of both CUB domains are represented by green spheres. The loop 151–157 between the two CUB domains, not visible in the electronic density, is depicted as a dotted line. VHH-H4 and VHH-I5 are represented as cartoons, colored in wheat and green respectively. The three CDR regions for both VHH are colored in purple (CDR1), blue (CDR2) and red (CDR3). (b) Close-up view on the interaction of the VHH-H4 CDR3 with the CUB1 domain (colored as in (a)). (c) A 2Fo-Fc electron density map contoured at 1.5σ of the interaction between K77 from the VHH-H4 framework and the calcium binding site of CUB2 (same color code as in (a)). (d) Close-up view on the interaction of the VHH-I5 CDR1 and CDR2 with the CUB2 domain (same color code as in (a)).

the complex, residues from its framework interact with the calcium binding site of CUB2. It is probable that the presence of VHH-I5 induces some conformational modification fostering these interactions, and further stabilizes the interface. The structural analysis also explains why VHH-I1 and I5, although belonging to the same family and sharing identical CDR2 and CDR3, have totally different behaviors. Asn32-Thr33 which play a critical role for the attachment of VHH-I5 to CUB2 are absent in VHH-I1 and replaced by Gln32-Ala33. Those two amino acids are also substituted in I2 and I4 which, like I1, are poor PCPE-1 binders with fast dissociation rates, probably because they cannot accommodate properly into the binding site.

We took advantage of VHH-I5 and VHH-H4 complementarity to create the biparatopic nanobody, diab-D1. The use of a flexible GS linker[40,41] enables a perfect binding of the diabody to its antigen and avidity enhances its affinity for PCPE-1, with a K_D of 0.32 nM and a very slow off-rate. But what is most striking is the fact that diab-D1 shows a remarkable ability to prevent PCPE-1 activity. Indeed, although VHHs H4 and I5 do not directly target the interaction zone

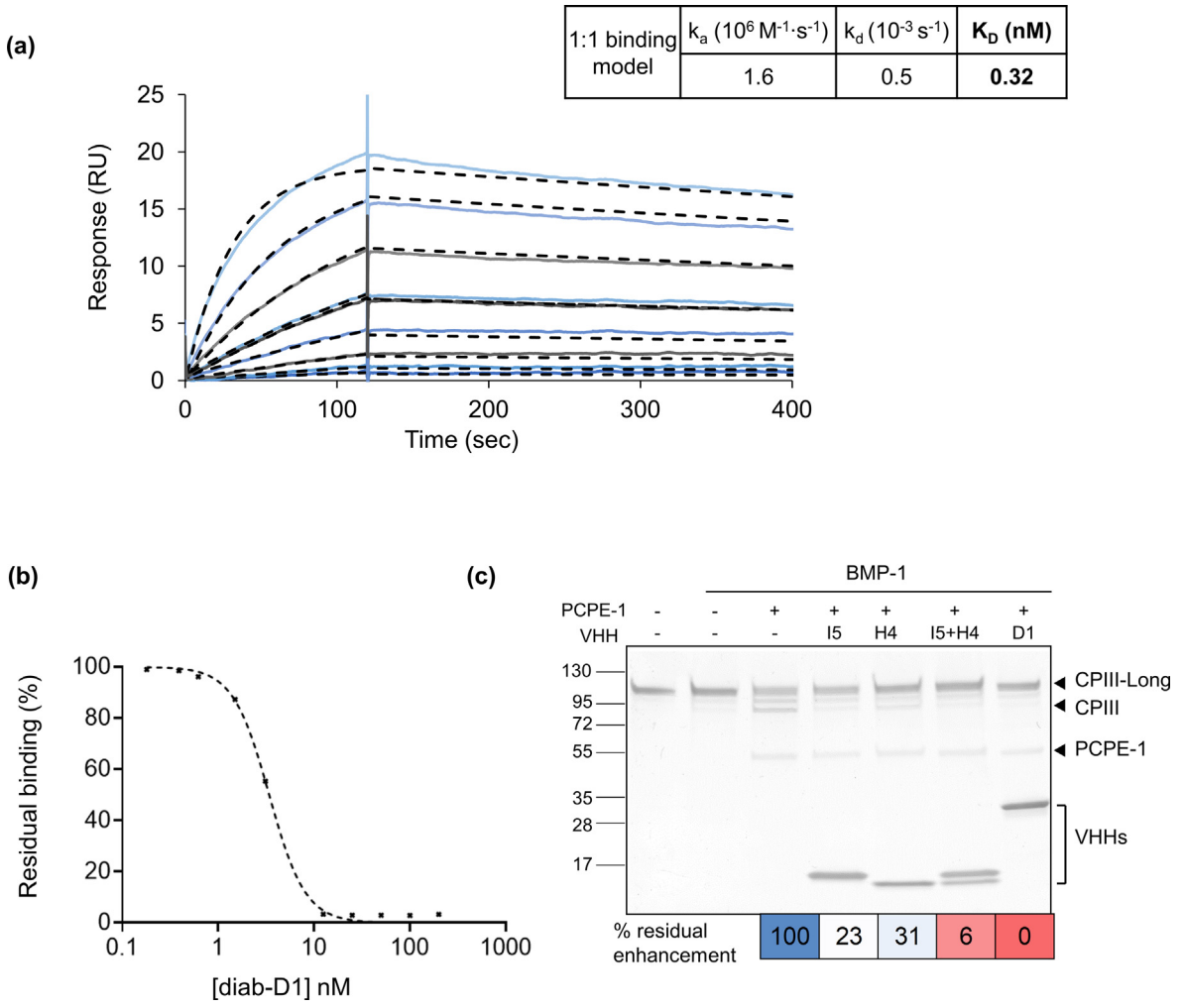

Figure 5. Characterization of diabody D1. (a) Increasing concentrations (0.16 to 20 nM) of diab-D1 were sequentially injected over immobilized PCPE-1 (110 RU). Fits (dotted line) were obtained with the 1:1 binding model (n = 2). (b) Competition experiments consisting of an injection of 2.5 nM PCPE-1 alone or in combination with increasing concentrations (0.2 to 200 nM) of diab-D1 over immobilized Mini-III (578 RU). Data are expressed as the % of residual binding normalized to PCPE-1 binding in the absence of diab-D1 (means ± ranges, n = 2). (c) CPIII-Long was incubated with BMP-1 and 75 nM PCPE-1 in the absence or presence of 2 μM VHH(s) for 1 h at 37 °C. Reaction products were analyzed by SDS-PAGE (4–20% polyacrylamide gel; non reducing conditions) and Coomassie Blue staining. % residual enhancement by PCPE-1 (compared to BMP-1 alone condition) is shown below the gel (quantification by densitometry, color coding according to % value). The gel is representative of n = 3 independent experiments.

between CUB1CUB2 and the C-propeptide of procollagen III (CP-III),[16] they are predicted to hinder the interaction with the latter by steric clashes, as can be seen in Figure 7.

Another advantage of using nanobodies is their high specificity. The nanobodies selected here do not cross-react with BMP-1, which also contains two consecutive CUB domains, nor with PCPE-2 although its CUB domains are 54% identical to those of PCPE-1. PCPE-2 has recently been described as having additional activities such as BTP inhibition[33] or promotion of HDL-cholesterol uptake by the scavenger receptor SRBI[42] and it is crucial that molecules dedicated to lowering procollagen processing have a minimal impact on PCPE-2 activity.

The efficient neutralization of procollagen processing in fibroblasts opens the possibility that diab-D1 could be used to control collagen fibril deposition in situations where overexpression of PCPE-1 is linked to fibrosis development. However, whether the observed diminution of extracellular procollagen processing will be translated into less abundant and better organized matrix deposition remains to be established. A major advantage of using diab-D1 to target PCPE-

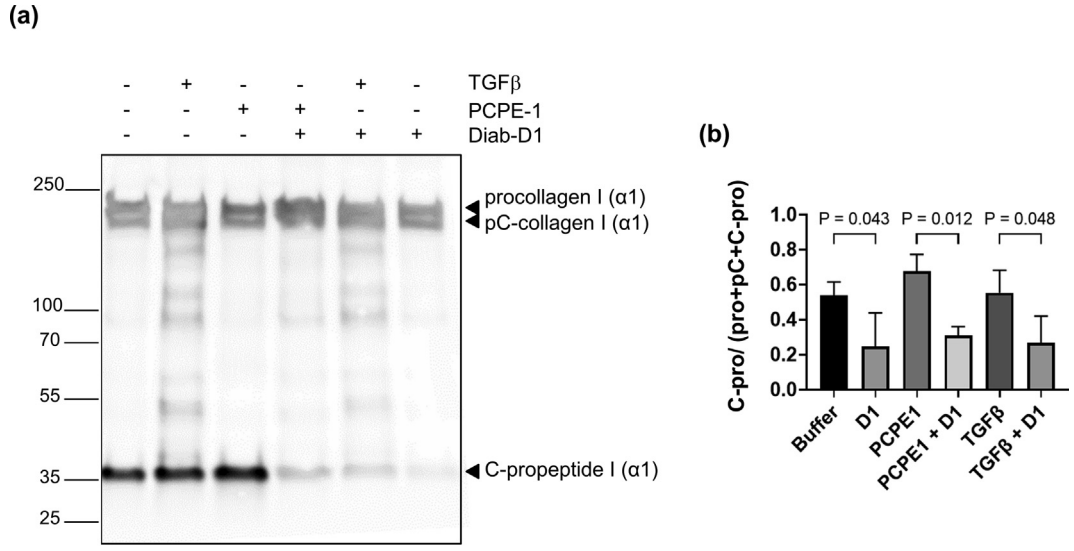

Figure 6. Inhibition of procollagen processing by diab-D1. (a) Human dermal fibroblasts were cultivated for 3 days in the absence or presence of TGFβ (1 ng/mL), PCPE-1 (5 μg/mL, 105 nM) and/or diab-D1 (15 μg/mL, 530 nM). Western blot analysis of the supernatant (equal amounts of medium, reducing conditions) using an antibody against the C-propeptide of procollagen I (LF41) (b) Quantification of the amount of released C-propeptide relative to all C-propeptide containing forms (densitometry). Means ± SD of 3 replicates are shown, conditions were compared using one-way ANOVA and Sidak test for multiple comparisons.

1, compared to directly targeting the protease, is that this would limit procollagen processing while maintaining the basal activity of the BTPs. This should enable the maturation of a minimum amount of collagen, which is essential for the proper repair of the injured tissue.[43]

One of the hallmarks of fibrosis is its slow evolution, which can take a long time to produce pathological effects on function. At present, there is an urgent need to develop sensitive and non-invasive techniques for the early detection and monitoring of fibrosis.[9,36,44,45] One such tool could be diab-D1 as its high affinity for PCPE-1 should enable the detection of areas of active collagen deposition, where PCPE-1 expression is often found to be up-regulated.[17,37,38,46] Indeed, nanobodies are easy to engineer and functionalize through coupling with fluorescent or radioactive labels. Their small size allows efficient tissue penetration and rapid clearance, leading to enhanced imaging resolution and reduced background signal and making them attractive tools for disease diagnosis and disease monitoring.[47–51]

In conclusion, we have developed a series of nanobodies targeting PCPE-1 with nanomolar or sub-nanomolar affinities and a remarkable ability to block PCPE-1 activity. They have strong potential for clinical applications, both as imaging tools and as modulators of collagen maturation or could even be designed as theranostic agents for the combined monitoring and treatment of fibrosis.

Material and Methods

Protein production and purification

Human PCPE-1 (hPCPE-1, native form or fused to a C-terminal 8-His tag), mini-procollagen III (with an N-terminal C-myc tag) and BMP-1 (with a C-terminal flag tag) were produced in HEK 293-EBNA cells and purified as previously described.[12,52,53] PCPE-1 CUB1 and CUB2 domains were generated through limited digestion of CUB1NTR and CUB2NTR constructs, as described by Kronenberg and colleagues.[13] CPIII-Long[15] and human PCPE-2 (fused to a N-terminal 6-His tag[33]) were produced by transient transfection of HEK 293-T and purified as described. Mini-I and Mini-II were produced by transient transfection of HEK 293-F and purified as described in.[35]

The CUB1CUB2 region of PCPE-1 (^{26}QTP---LPRGT^{277}, starting at the first residue of the mature protein after signal peptide removal) was used as the antigen for nanobody generation. It was cloned into the pHLsec vector in fusion with a 6-His tag and a HRV-3C recognition sequence at the N-terminus, giving the following N-terminal sequence after 3C cleavage: **GPAG**QTP. CUB1CUB2 was transiently expressed in 293-F cells, grown at 37 °C, 125 rpm with 8% CO_2 in FreeStyle™ 293 expression medium (Gibco) following the procedure described in Pulido et al.[16] Then, CUB1CUB2 was purified on a Ni-excel

column (5 ml; Cytiva) followed by HRV-3C protease treatment (1/30 w/w) at 4 °C overnight to eliminate the 6-His tag. The resulting protein was loaded on a HiLoad 16/600 Superdex 75 pg SEC (size exclusion chromatography) column (Cytiva) equilibrated in 20 mM HEPES pH 7.4, 0.3 M NaCl, 2.5 mM $CaCl_2$. Fractions containing the purified protein were pooled, concentrated (Amicon 10 KDa, Merck) and stored at −80 °C in the same buffer. Protein concentration was determined using a Nanodrop 2000 spectrophotometer (Thermo Scientific) and extinction coefficients computed from Expasy ProtParam tool.[54]

For bio-panning and phage ELISA, a biotinylated form of CUB1CUB2 was generated. The sequence of the CUB1CUB2 domain was cloned into pHL-Avitag3[55] between the EcoRI and KpnI restriction sites and expressed by transient transfection in 293-T cells as in.[15] After a first purification step onto Immobilized Metal-ion Affinity chromatography (Qiagen), 60 μM Avitagged CUB1CUB2 was biotinylated using 1 μM GST-BirA (Biotin-protein

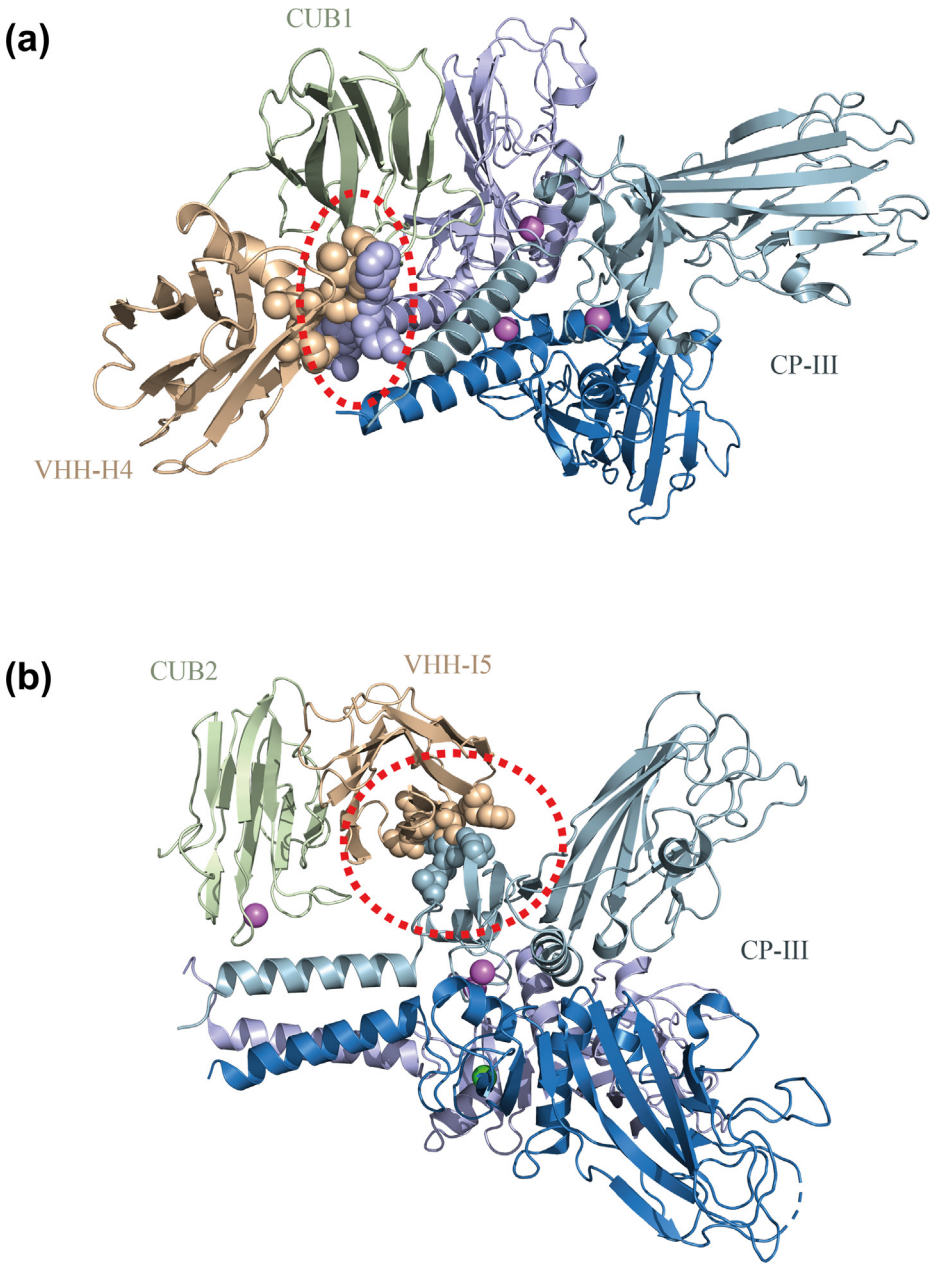

Figure 7. Comparison of the complexes formed by CUB1CUB2/VHH-H4/VHH-I5 (9EN2) and CUB1CUB2/CP-III (6FZV). The crystal structures of the two complexes were superimposed and aligned (a) on CUB1 (b) on CUB2. In both cases, steric clashes (zone circled by a dotted line) hinder proper interaction of CUB1CUB2 with CP-III. The 3 chains of CP-III are depicted in shades of blue, CUB domains in light green and VHHs in gold.

ligase) in 50 mM bicine, 300 mM potassium glutamate pH 8.3 supplemented with 10 mM ATP (Sigma) and 50 μM d-biotine (Sigma) during 5 h at 30 °C. GST-BirA in pGex vector was a generous gift from Dr. Y. Zhao (STRUBI, Oxford University, UK) and was expressed in *E. Coli BL21(DE3)pLysS* and purified following the procedure of O'Callaghan.[56]

GST-BirA and the remaining biotin were removed by SEC on a HiLoad 16/600 Superdex 75 pg column in 20 mM HEPES pH 7.4, 0.3 M NaCl. The biotinylation level was evaluated by loading on Streptavidin Sepharose and analyzing the flow through by SDS-PAGE, and was estimated to be superior to 95%.

Generation of VHHs by immunization of a llama

Immune-derived nanobodies were generated by the AFMB facility (Marseille, France). Briefly, immunization of a *Llama glama* was achieved through five successive injections of 1 mg of purified CUB1CUB2 at one-week intervals. Blood was collected on day 39 and the nanobody library was generated as previously described.[57] Phages displaying CUB1CUB2-specific VHHs were enriched after two rounds of bio-panning on 50 nM biotinylated CUB1CUB2. After the last round, 48 phagemid clones were picked and binding to human PCPE-1 was determined by phage ELISA. The sequences of positive clones were analyzed and aligned using ESPript 3.0.[58] Eight nanobodies were chosen for further characterization.

Generation of synthetic VHHs

Synthetic nanobodies were generated by Hybrigenics Services SAS (Evry, France). Three rounds of bio-panning using the synthetic hsd2ab VHH library[20] were carried out on biotinylated CUB1CUB2. At the end of the selection process, 90 phagemid clones were randomly picked and an ELISA-binding screen was performed leading to 24 unique clones. A second round of ELISA screen was performed, using CUB1NTR as the antigen, to select clones able to interact with the CUB1 domain of human PCPE-1. After sequence analysis, ten nanobodies were chosen for further characterization.

Production and purification of nanobodies

Synthetic VHHs were cloned into the pHEN2 vector in fusion with the *pelB* signal sequence and, at the C-terminus, a 6-His tag followed by 3c-myc tags. VHH-H4 and -H10 were later cloned into the pET29b(+) vector, in fusion with the *pelB* signal sequence and a 6-His tag at the C-terminus. Llama VHHs were cloned into the pHEN6 vector downstream the *pelB* sequence and fused to a C-terminal 6-His tag. The bivalent nanobody construct was prepared in the pET29b (+) vector as follows. Llama nanobody VHH-I5 was amplified by PCR with a NotI restriction site and a GS linker (GSGSGSGSGSGSGGS, called GS_8 below) sequence added to its N-terminus. GS_8-VHH-I5 was then cloned downstream of VHH-H4 in pET29b(+) by NotI/XhoI digestion to yield the bivalent nanobody VHH-H4-GS_8-VHH-I5 (diab-D1).

The plasmids were transformed into the T7 express *E. coli* strain (NEB) and protein expression was induced by 1 mM IPTG (β-D-1-thio galactopyranoside) at OD600 = 0.8. Cells were grown overnight at 28 °C in Terrific Broth medium supplemented with 0.1% glucose, harvested by centrifugation at 4000 rpm for 15 min at 4 °C and resuspended in TES buffer (200 mM Tris HCl pH 8.0, 500 mM Sucrose, 50 nM EDTA). Periplasmic extracts were prepared by the osmotic shock method[57] and soluble VHHs were purified by nickel-affinity chromatography (Qiagen) and SEC (Hiload 16/600 Superdex 75 pg; Cytiva) in 20 mM HEPES, 0.3 M NaCl pH 7.4.

VHH-I5 and -H4 were also cloned for expression in the pHEN6 plasmid with a C-terminal Sortase recognition site (LPETG) and a 6-His tag (generous gift from Dr. Leo Hanke, Karolinska Institute, Stockholm, Sweden), and produced and purified as described in.[59] In parallel, the Sortase A 5M (SrtA 5M) required for biotinylation was cloned for expression in the pET30b plasmid (gift from Hidde Ploegh[60]; Addgene plasmid #51140; https://n2t.net/addgene:51140; RRID:Addgene_51140), with a C-terminal 6-His tag, and purified according to Chen et al.[61] Nanobodies harboring the Sortase recognition site were biotinylated on their C-terminus using 50 μM SrtA 5M and 200 μM GGGK-biotin (Covalab) in 50 mM HEPES pH 7.5, 150 mM NaCl, 10 mM $CaCl_2$ for 2 h at 25 °C.[59] SrtA 5M and unreacted VHHs were eliminated on Ni-NTA resin (Qiagen) and excess GGGK-biotin peptide was removed using Zeba spin desalting columns 7 K MWCO (Thermo Fisher).

SPR experiments

Surface plasmon resonance experiments were performed using a Biacore T200 apparatus (Cytiva). Protein ligands were immobilized on the carboxymethylated dextran surface of CM5 sensor chips using amine coupling chemistry. Prior to immobilization, ligands were diluted in 10 mM HEPES pH 7.4 for PCPE-1 or in 10 mM sodium acetate pH 4.5 for mini-procollagen III and streptavidin (Calbiochem). Soluble analytes were diluted in running buffer (10 mM HEPES pH 7.4, 0.15 M NaCl, 5 mM $CaCl_2$, 0.05% P20) and injected at a flow rate of 30 or 50 μL/min. Competition assays as well as epitope binning and kinetic experiments were all carried out at 25 °C. Regeneration was performed with successive 30 sec pulses of 2 M guanidinium

chloride and 0.5 M EDTA. For the competition experiments involving two analytes (Figures 2a, 3a and S6), the "mix and inject" mode of the Biacore T200 was used: the two analytes were prepared separately, mixed and allowed to form a complex for 200 sec, before injection on the surface. Sensorgrams were analyzed using Biacore T200 evaluation software (v3.2.1). Model fitting was carried out using the 1:1 binding, heterogeneous ligand or steady-state models. IC_{50}s were determined by nonlinear regression using GraphPad Prism (v8.2.1).

Activity assays

To characterize the effects of VHHs on PCPE-1 activity, 400 nM of CPIII-Long were incubated for 1 h at 37 °C with 3 nM BMP-1 and 75 nM PCPE-1 (when present) in the presence or absence of 2 μM nanobody in the following buffer: 20 mM HEPES pH 7.4, 0.15 M NaCl, 5 mM $CaCl_2$, 0.02% *n*-octyl-β-D-glucopyranoside. The samples were analyzed by SDS-PAGE using 4–20% gradient gels (Criterion; Biorad) and Instant Blue staining (Euromedex). The activation level by PCPE-1 was evaluated as the ratio of C-propeptide band intensity to all CPIII-Long (cleaved and uncleaved) band intensities after normalization with the BMP-1 alone condition using ImageQuant TL software (Cytiva).

Cell culture

Primary human dermal fibroblasts were obtained from the Cell and Tissue Bank of Edouard Herriot Hospital (Lyon, France, permanent authorization of the French Ministry of Higher Education, Research and Innovation AC-2019-3476), after isolation in accordance with ethical regulations by outgrowths of explant cultures from the breast skin of a healthy female donor (aged 32 years).

Fibroblasts were grown in DMEM AQ™ medium (Merck) with 10% Fetal Bovine Serum (FBS, Eurobio), 50 $\mu g \cdot mL^{-1}$ ascorbic acid (Sigma) and 1% AAS (Antibiotic-antimycotic solution; Thermo Fisher) and incubated at 37 °C with 5% CO2. When the cells reached 70% of confluency, FBS was removed and serum-free medium containing PCPE-1 (5 $\mu g \cdot mL^{-1}$, 105 nM) or TGF-beta (1 $ng \cdot mL^{-1}$, Peprotech) with or without 15 $\mu g \cdot mL^{-1}$ (530 nM) nanobody was added. Cells were maintained in this medium for 72 h after which the supernatants were collected and centrifuged at 10,000*g*. Equal amounts of samples were analyzed by SDS-PAGE on stain-free 4–20% gradient gels (Criterion; Bio-Rad). After migration, gels were activated (1 min UV exposure) and imaged (FX Fusion CCD camera, Vilber Lourmat) to confirm rough equal loading. Proteins were then electrotransferred to PVDF membranes using 10 mM CAPS buffer (pH 11) supplemented with 10% ethanol, blocked with 10% skimmed milk in PBS and procollagen I processing was analyzed using an anti-C-propeptide antibody (LF41, kind gift of Dr. Larry W. Fisher, Bethesda, USA).[62] Relative quantification (band intensities) of the amount of released C-propeptide relative to all C-propeptide-containing collagen forms (procollagen + pC-collagen + C-propeptide) was performed by densitometry using ImageQuant TL software (Cytiva).

Rat cardiac fibroblasts were extracted[63] and processed as above, except that the supernatants were collected 2 days after serum deprivation.

Primary cells were checked for mycoplasma contamination (MycoAlert, Lonza).

CUB1CUB2–nanobodies complex purification

For crystallogenesis experiments, 70 μmol of CUB1CUB2, VHH-H4 and VHH-I5 were mixed at room temperature in 2 mL during 30 min. Then, the complex was loaded onto a HiLoad 16/600 Superdex 200 pg column (Cytiva) equilibrated in 20 mM HEPES pH 7.4, 125 mM NaCl, 2.5 mM $CaCl_2$. The CUB1CUB2–VHH-H4–VHH-I5 complex eluted as a single peak. Fractions were pooled and concentrated to 7 $mg \cdot mL^{-1}$. DLS analysis showed a single monodisperse population.

The complex formed by CUB1CUB2 and diab-D1 was isolated using the same protocol.

Crystallization, data collection and processing

Crystallization conditions were screened at 19 °C using the sitting-drop vapor-diffusion method and commercial kits from Hampton Research, Molecular Dimensions Limited and Qiagen in 96-well plates (MRC plates SwissCi) with a Mosquito nanodispenser STP Labtech. Crystals of the CUB1CUB2–VHH-E9–VHH-E10 complex were obtained at 7 $mg \cdot mL^{-1}$ in 10% PEG 8000, 50 mM L-argininamide dihydrochloride, 50 mM spermine, 50 mM sodium cacodylate pH 6.5 and 50 mM potassium chloride. Crystals were cryoprotected in 50% glycerol, and flash-frozen in liquid nitrogen.

Diffraction data were collected at 100 K on beamline PROXIMA-1 at Synchrotron SOLEIL. The data were processed using the XDS[64] and AIMLESS programs of the CCP4 suite.[65] Phases were determined by molecular replacement using PHASER[66] with four search models. Individual CUB domains were extracted from the PDB structure **6FZV**. For both VHH-H4 and I5, corresponding domains were extracted from the PDB **6SGE** and **6V80** structures respectively, and the three CDR

regions of each VHH were removed. Manual rebuilding and refinement were done using COOT[67] and Refmac. Surfaces were calculated using the PISA webserver (https://www.ebi.ac.uk/pdbe/prot_int/pistart.html).[34] Figures were generated using PyMOL (https://www.pymol.org). Data collection and refinement statistics are given in Table 2.

Statistical analyses

Statistical analyses were performed using Graphpad Prism v8.2.1 or 9.5.0.

Accession numbers

Coordinates and structure factors have been deposited in the Protein Data Bank under the accession number (PDB ID) **9EN2** (PCPE-1 CUB1-CUB2 domains in complex with nanobodies VHH-H4 and VHH-I5).

Funding

This work was supported by the French Government [ANR grant No. ANR-17-CE14-0033 and ANR-21-CE11-0020]; the Centre National de la Recherche Scientifique; the University of Lyon.

CRediT authorship contribution statement

Priscillia Lagoutte: Writing – review & editing, Writing – original draft, Visualization, Validation, Methodology, Investigation, Formal analysis, Conceptualization. **Jean-Marie Bourhis:** Writing – review & editing, Visualization, Validation, Investigation, Formal analysis, Data curation. **Natacha Mariano:** Writing – review & editing, Validation, Investigation. **Virginie Gueguen-Chaignon:** Writing – review & editing, Validation, Investigation, Formal analysis. **David Vandroux:** Writing – review & editing, Resources, Funding acquisition, Conceptualization. **Catherine Moali:** Writing – review & editing, Validation, Supervision, Methodology, Investigation, Funding acquisition, Conceptualization. **Sandrine Vadon-Le Goff:** Writing – review & editing, Writing – original draft, Visualization, Validation, Supervision, Project administration, Methodology, Investigation, Funding acquisition, Formal analysis, Conceptualization.

DECLARATION OF COMPETING INTEREST

The authors declare the following financial interests/personal relationships which may be considered as potential competing interests: 'DV is the former CEO of NVH Medicinal. PL, SVLG, CM and DV have filed a patent regarding the nanobodies described in this study (PCT/FR2023/050369). The authors declare that they have no other competing financial interests'.

Acknowledgement

We acknowledge SOLEIL for the provision of synchrotron radiation facilities and we would like to thank Pierre Legrand for assistance in using "PX-1 beamline".
We thank Juliette Hof for the drawing of the llama used in the graphical abstract and Fig. 1. We also acknowledge the contribution of Antoine Duvillard (LBTI, CNRS-University of Lyon) to the optimization of the sortagging of the VHHs, and we warmly thank Francine Gerard Barragia for her contribution to sample transportation between the Lyon and Grenoble labs.

Appendix A. Supplementary material

Supplementary material to this article can be found online at https://doi.org/10.1016/j.jmb.2024.168667.

Received 3 April 2024;
Accepted 13 June 2024;
Available online 18 June 2024

Keywords:
binder;
VHH;
proteolysis;
collagen;
fibrosis

Abbreviations:
PCPE, procollagen C-proteinase enhancer; BMP-1, bone morphogenetic protein-1; BTPs, BMP-1/tolloid-like proteinases; VHH, variable heavy-chain domains of heavy-chain only antibodies; CUB, Complement-Uegf-BMP-1; NTR, netrin-like

References

1. Kadler, K.E., Hojima, Y., Prockop, D.J., (1987). Assembly of collagen fibrils de novo by cleavage of the type I pC-collagen with procollagen C-proteinase. Assay of critical concentration demonstrates that collagen self-assembly is

a classical example of an entropy-driven process. *J. Biol. Chem.* **262**, 15696–15701.
2. Revell, C.K., Jensen, O.E., Shearer, T., Lu, Y., Holmes, D. F., Kadler, K.E., (2021). Collagen fibril assembly: New approaches to unanswered questions. *Matrix Biol. Plus* **12**, 100079.
3. Hulmes, D.J.S., (2019). Roles of the procollagen C-propeptides in health and disease. *Essays Biochem.* **63**, 313–323.
4. Wynn, T.A., Ramalingam, T.R., (2012). Mechanisms of fibrosis: Therapeutic translation for fibrotic disease. *Nature Med.* **18**, 1028–1040.
5. Henderson, N.C., Rieder, F., Wynn, T.A., (2020). Fibrosis: from mechanisms to medicines. *Nature* **587**, 555–566.
6. Zhao, M., Wang, L., Wang, M., Zhou, S., Lu, Y., Cui, H., Racanelli, A.C., Zhang, L., Ye, T., Ding, B., Zhang, B., Yang, J., Yao, Y., (2022). Targeting fibrosis, mechanisms and clinical trials. *Signal Transduct. Target. Ther.* **7**, 206.
7. Nie, X., Qian, L., Sun, R., Huang, B., Dong, X., Xiao, Q., Zhang, Q., Lu, T., Yue, L., Chen, S., Li, X., Sun, Y., Li, L., Xu, L., Li, Y., Yang, M., Xue, Z., Liang, S., Ding, X., Yuan, C., Peng, L., Liu, W., Yi, X., Lyu, M., Xiao, G., Xu, X., Ge, W., He, J., Fan, J., Wu, J., Luo, M., Chang, X., Pan, H., Cai, X., Zhou, J., Yu, J., Gao, H., Xie, M., Wang, S., Ruan, G., Chen, H., Su, H., Mei, H., Luo, D., Zhao, D., Xu, F., Zhu, Y., Xia, J., Hu, Y., Guo, T., (2021). Multi-organ proteomic landscape of COVID-19 autopsies. *Cell* **184**, 775–791.
8. Zhao, X., Kwan, J.Y.Y., Yip, K., Liu, P.P., Liu, F.F., (2020). Targeting metabolic dysregulation for fibrosis therapy. *Nature Rev. Drug Discov.* **19**, 57–75.
9. Walraven, M., Hinz, B., (2018). Therapeutic approaches to control tissue repair and fibrosis: Extracellular matrix as a game changer. *Matrix Biol.* **71–72**, 205–224.
10. Vadon-Le Goff, S., Hulmes, D.J.S., Moali, C., (2015). BMP-1/tolloid-like proteinases synchronize matrix assembly with growth factor activation to promote morphogenesis and tissue remodeling. *Matrix Biol.* **44–46**, 14–23.
11. Adar, R., Kessler, E., Goldberg, B., (1986). Evidence for a protein that enhances the activity of type I Procollagen C-Proteinase. *Collagen Relat. Res.* **6**, 267–277.
12. Moali, C., Font, B., Ruggiero, F., Eichenberger, D., Rousselle, P., François, V., Oldberg, Å., Bruckner-Tuderman, L., Hulmes, D.J.S.S., (2005). Substrate-specific modulation of a multisubstrate proteinase: C-terminal processing of fibrillar procollagens is the only BMP-1-dependent activity to be enhanced by PCPE-1. *J. Biol. Chem.* **280**, 24188–24194.
13. Kronenberg, D., Vadon-Le Goff, S., Bourhis, J.-M., Font, B., Eichenberger, D., Hulmes, D.J.S., Moali, C., (2009). Strong cooperativity and loose geometry between CUB domains are the basis for procollagen C-proteinase enhancer activity. *J. Biol. Chem.* **284**, 33437–33446.
14. Vadon-Le Goff, S., Kronenberg, D., Bourhis, J.-M., Bijakowski, C., Raynal, N., Ruggiero, F., Farndale, R.W., Stöcker, W., Hulmes, D.J.S., Moali, C., (2011). Procollagen C-proteinase enhancer stimulates procollagen processing by binding to the C-propeptide region only. *J. Biol. Chem.* **286**, 38932–38938.
15. Bourhis, J.-M., Vadon-Le Goff, S., Afrache, H., Mariano, N., Kronenberg, D., Thielens, N., Moali, C., Hulmes, D.J.S., (2013). Procollagen C-proteinase enhancer grasps the stalk of the C-propeptide trimer to boost collagen precursor maturation. *Proc. Natl. Acad. Sci. U. S. A.* **110**, 6394–6399.
16. Pulido, D., Sharma, U., Vadon-Le Goff, S., Hussain, S.A., Cordes, S., Mariano, N., Bettler, E., Moali, C., Aghajari, N., Hohenester, E., Hulmes, D.J.S., (2018). Structural basis for the acceleration of procollagen processing by Procollagen C-Proteinase Enhancer-1. *Structure* **26**, 1384–1392.e3.
17. Lagoutte, P., Bettler, E., Vadon-Le Goff, S., Moali, C., (2021). Procollagen C-proteinase enhancer-1 (PCPE-1), a potential biomarker and therapeutic target for fibrosis. *Matrix Biol. Plus* **11**, 100062.
18. Hamers-Casterman, C., Atarchouch, T., Muyldermans, S., Robinson, G., Hamers, C., Bajyana Songa, E., Bendahman, N., Hamers, R., (1993). Naturally occurring antibodies devoid of light chains. *Nature* **363**, 446–448.
19. Muyldermans, S., (2021). A guide to: generation and design of nanobodies. *FEBS J.* **288**, 2084–2102.
20. Moutel, S., Bery, N., Bernard, V., Keller, L., Lemesre, E., De Marco, A., Ligat, L., Rain, J.C., Favre, G., Olichon, A., Perez, F., (2016). NaLi-H1: A universal synthetic library of humanized nanobodies providing highly functional antibodies and intrabodies. *Elife* **5**, e16228.
21. Zimmermann, I., Egloff, P., Hutter, C.A., Arnold, F.M., Stohler, P., Bocquet, N., Hug, M.N., Huber, S., Siegrist, M., Hetemann, L., Gera, J., Gmür, S., Spies, P., Gygax, D., Geertsma, E.R., Dawson, R.J., Seeger, M.A., (2018). Synthetic single domain antibodies for the conformational trapping of membrane proteins. *Elife* **7**, e34317.
22. Wilton, E.E., Opyr, M.P., Kailasam, S., Kothe, R.F., Wieden, H.J., (2018). SdAb-DB: The single domain antibody database. *ACS Synth. Biol.* **7**, 2480–2484.
23. Jin, B.K., Odongo, S., Radwanska, M., Magez, S., (2023). Nanobodies: A review of generation, diagnostics and therapeutics. *Int. J. Mol. Sci.* **24**, 5994.
24. Uchański, T., Pardon, E., Steyaert, J., (2020). Nanobodies to study protein conformational states. *Curr. Opin. Struct. Biol.* **60**, 117–123.
25. Pain, C., Dumont, J., Dumoulin, M., (2015). Camelid single-domain antibody fragments: Uses and prospects to investigate protein misfolding and aggregation, and to treat diseases associated with these phenomena. *Biochimie* **111**, 82–106.
26. Zhang, L., Zang, B., Huang, C., Ren, J., Jia, L., (2019). One-step preparation of a VHH-based immunoadsorbent for the extracorporeal removal of β2-microglobulin. *Molecules* **24**, 219.
27. He, J., Ma, S., Wu, S., Xu, J., Tian, J., Li, J., Gee, S.J., Hammock, B.D., Li, Q.X., Xu, T., (2020). Construction of immunomagnetic particles with high stability in stringent conditions by site-directed immobilization of multivalent nanobodies onto bacterial magnetic particles for the environmental detection of tetrabromobisphenol-a. *Anal. Chem.* **92**, 1114–1121.
28. Scully, M., Cataland, S.R., Peyvandi, F., Coppo, P., Knöbl, P., Kremer Hovinga, J.A., Metjian, A., de la Rubia, J., Pavenski, K., Callewaert, F., Biswas, D., De Winter, H., Zeldin, R.K., (2019). Caplacizumab treatment for acquired thrombotic thrombocytopenic purpura. *N. Engl. J. Med.* **380**, 335–346.
29. Keam, S.J., (2023). Ozoralizumab: First approval. *Drugs* **83**, 87–92.
30. Naidoo, D.B., Chuturgoon, A.A., (2023). The potential of nanobodies for COVID - 19 diagnostics and therapeutics. *Mol. Diagn. Ther.* **27**, 193–226.
31. Huo, J., Le Bas, A., Ruza, R.R., Duyvesteyn, H.M.E., Mikolajek, H., Malinauskas, T., Tan, T.K., Rijal, P.,

Dumoux, M., Ward, P.N., Ren, J., Zhou, D., Harrison, P.J., Weckener, M., Clare, D.K., Vogirala, V.K., Radecke, J., Moynié, L., Zhao, Y., Gilbert-Jaramillo, J., Knight, M.L., Tree, J.A., Buttigieg, K.R., Coombes, N., Elmore, M.J., Carroll, M.W., Carrique, L., Shah, P.N.M., James, W., Townsend, A.R., Stuart, D.I., Owens, R.J., Naismith, J.H., (2020). Neutralizing nanobodies bind SARS-CoV-2 spike RBD and block interaction with ACE2. *Nature Struct. Mol. Biol.* **27**, 846–854.

32. Wagner, T.R., Blaess, S., Leske, I.B., Frecot, D.I., Gramlich, M., Traenkle, B., Kaiser, P.D., Seyfried, D., Maier, S., Rezza, A., Sônego, F., Thiam, K., Pezzana, S., Zeck, A., Gouttefangeas, C., Scholz, A.M., Nueske, S., Maurer, A., Kneilling, M., Pichler, B.J., Sonanini, D., Rothbauer, U., (2023). Two birds with one stone: human SIRPα nanobodies for functional modulation and in vivo imaging of myeloid cells. *Front. Immunol.* **14**, 1264179.
33. Vadon-Le Goff, S., Tessier, A., Napoli, M., Dieryckx, C., Bauer, J., Dussoyer, M., Lagoutte, P., Peyronnel, C., Essayan, L., Kleiser, S., Tueni, N., Bettler, E., Mariano, N., Errazuriz-Cerda, E., Fruchart Gaillard, C., Ruggiero, F., Becker-Pauly, C., Allain, J.M., Bruckner-Tuderman, L., Nyström, A., Moali, C., (2023). Identification of PCPE-2 as the endogenous specific inhibitor of human BMP-1/tolloid-like proteinases. *Nature Commun.* **14**, 8020.
34. Krissinel, E., Henrick, K., (2007). Inference of Macromolecular Assemblies from Crystalline State. *J. Mol. Biol.* **372**, 774–797.
35. Mariano, N., Dieryckx, C., Tessier, A., Vincourt, J.-B., Vadon-Le Goff, S., Moali, C., (2023). Production of recombinant heterotrimeric mini-procollagen I and homotrimeric mini-procollagen II reveals new cleavage sites for BMP-1. *bioRxiv*. 2022.11.10.516045.
36. Karsdal, M.A., Daniels, S.J., Holm Nielsen, S., Bager, C., Rasmussen, D.G.K., Loomba, R., Surabattula, R., Villesen, I.F., Luo, Y., Shevell, D., Gudmann, N.S., Nielsen, M.J., George, J., Christian, R., Leeming, D.J., Schuppan, D., (2020). Collagen biology and non-invasive biomarkers of liver fibrosis. *Liver Int.* **40**, 736–750.
37. Hassoun, E., Safrin, M., Ziv, H., Pri-Chen, S., Kessler, E., (2016). Procollagen C-Proteinase Enhancer 1 (PCPE-1) as a plasma marker of muscle and liver fibrosis in mice. *PLoS One* **11**, e0159606.
38. Sansilvestri, P., Id, M., Duvivier, V., Bertin, F., Provost, N., Id, A.H., Hubert, E., Gonzalez, A., Tupinon-, I., Paradis, V., Delerive, P., (2022). Procollagen C-Proteinase Enhancer-1 (PCPE-1) deficiency in mice reduces liver fibrosis but not NASH progression. *PLoS One* **17**, e0263828.
39. Koenig, P.A., Das, H., Liu, H., Kümmerer, B.M., Gohr, F.N., Jenster, L.M., Schiffelers, L.D.J., Tesfamariam, Y.M., Uchima, M., Wuerth, J.D., Gatterdam, K., Ruetalo, N., Christensen, M.H., Fandrey, C.I., Normann, S., Tödtmann, J.M.P., Pritzl, S., Hanke, L., Boos, J., Yuan, M., Zhu, X., Schmid-Burgk, J.L., Kato, H., Schindler, M., Wilson, I.A., Geyer, M., Ludwig, K.U., Hällberg, B.M., Wu, N.C., Schmidt, F.I., (2021). Structure-guided multivalent nanobodies block SARS-CoV-2 infection and suppress mutational escape.. *Science* **371**, eabe6230.
40. Pymm, P., Redmond, S.J., Dolezal, O., Mordant, F., Lopez, E., Cooney, J.P., Davidson, K.C., Haycroft, E.R., Tan, C. W., Seneviratna, R., Grimley, S.L., Purcell, D.F.J., Kent, S. J., Wheatley, A.K., Wang, L.F., Leis, A., Glukhova, A., Pellegrini, M., Chung, A.W., Subbarao, K., Uldrich, A.P., Tham, Godfrey, D.I., Gherardin, N.A., (2022). Biparatopic nanobodies targeting the receptor binding domain efficiently neutralize SARS-CoV-2. *iScience* **25**, 105259.
41. Klein, J.S., Jiang, S., Galimidi, R.P., Keeffe, J.R., Bjorkman, P.J., Regan, L., (2014). Design and characterization of structured protein linkers with differing flexibilities. *Protein Eng. Des. Sel.* **27**, 325–330.
42. Xu, H., Thomas, M.J., Kaul, S., Kallinger, R., Ouweneel, A. B., Maruko, E., Oussaada, S.M., Jongejan, A., Cense, H. A., Nieuwdorp, M., Serlie, M.J., Goldberg, I.J., Civelek, M., Parks, B.W., Lusis, A.J., Knaack, D., Schill, R.L., May, S. C., Reho, J.J., Grobe, J.L., Gantner, B., Sahoo, D., Sorci-thomas, M.G., (2021). PCPE2, a novel extracellular matrix protein, regulates adipocyte SR-BI–mediated high-density lipoprotein uptake. *Arterioscler. Thromb. Vasc. Biol.* **41**, 2708–2725.
43. Muir, A.M., Massoudi, D., Nguyen, N., Keene, D.R., Lee, S. J., Birk, D.E., Davidson, J.M., Marinkovich, M.P., Greenspan, D.S., (2016). BMP1-like proteinases are essential to the structure and wound healing of skin. *Matrix Biol.* **56**, 114–131.
44. Montesi, S.B., Désogère, P., Fuchs, B.C., Caravan, P., (2019). Molecular imaging of fibrosis: Recent advances and future directions. *J. Clin. Invest.* **129**, 24–33.
45. Motiwala, S.R., Gaggin, H.K., (2016). Biomarkers to Predict Reverse Remodeling and Myocardial Recovery in Heart Failure. *Curr. Heart Fail. Rep.* **13**, 207–218.
46. Lagoutte, P., Oudot, A., Dussoyer, M., Goncalves, V., Bouchot, O., Vandroux, D., Bellaye, P., Moali, C., (2021). Procollagen C-Proteinase Enhancer 1 (PCPE-1) is a marker of myocardial fibrosis and impaired cardiac function in a murine model of pressure overload. *bioRxiv*. 2021.03.05.434071.
47. Harmand, T.J., Islam, A., Pishesha, N., Ploegh, H.L., (2021). Nanobodies as in vivo, non-invasive, imaging agents. *RSC Chem. Biol.* **2**, 685–701.
48. Renard, E., Camps, E.C., Canovas, C., Kip, A., Gotthardt, M., Rijpkema, M., Denat, F., Goncalves, V., van Lith, S.A. M., (2021). Site-specific dual-labeling of a VHH with a chelator and a photosensitizer for nuclear imaging and targeted photodynamic therapy of EGFR-positive tumors. *Cancers (Basel)* **13**, 428.
49. Jailkhani, N., Ingram, J.R., Rashidian, M., Rickelt, S., Tian, C., Mak, H., Jiang, Z., Ploegh, H.L., Hynes, R.O., (2019). Noninvasive imaging of tumor progression, metastasis, and fibrosis using a nanobody targeting the extracellular matrix. *Proc. Natl. Acad. Sci. U. S. A.* **116**, 14181–14190.
50. Jailkhani, N., Clauser, K.R., Mak, H.H., Rickelt, S., Tian, C., Whittaker, C.A., Tanabe, K.K., Purdy, S.R., Carr, S.A., Hynes, R.O., (2023). Proteomic profiling of extracellular matrix components from patient metastases identifies consistently elevated proteins for developing nanobodies that target primary tumors and metastases. *Cancer Res.* **83**, 2052–2065.
51. Cawez, F., Mercuri, P.S., Morales-Yãnez, F.J., Maalouf, R., Vandevenne, M., Kerff, F., Guérin, V., Mainil, J., Thiry, D., Saulmont, M., Vanderplasschen, A., Lafaye, P., Aymé, G., Bogaerts, P., Dumoulin, M., Galleni, M., (2023). Development of nanobodies as theranostic agents against CMY-2-like class C beta-lactamases. *Antimicrob. Agents Chemother.* **67**, 1–19.
52. Blanc, G., Font, B., Eichenberger, D., Moreau, C., Ricard-Blum, S., Hulmes, D.J.S., Moali, C., (2007). Insights into

how CUB domains can exert specific functions while sharing a common fold: Conserved and specific features of the CUB1 domain contribute to the molecular basis of procollagen C-proteinase enhancer-1 activity. *J. Biol. Chem.* **282**, 16924–16933.
53. Hung, C.-W., Koudelka, T., Anastasi, C., Becker, A., Moali, C., Tholey, A., (2016). Characterization of post-translational modifications in full-length human BMP-1 confirms the presence of a rare vicinal disulfide linkage in the catalytic domain and highlights novel features of the EGF domain. *J. Proteomics* **138**, 136–145.
54. Duvaud, S., Gabella, C., Lisacek, F., Stockinger, H., Ioannidis, V., Durinx, C., (2021). Expasy, the Swiss Bioinformatics Resource Portal, as designed by its users. *Nucleic Acids Res.* **49**, W216–W227.
55. Aricescu, A.R., Lu, W., Jones, E.Y., (2006). A time- and cost-efficient system for high-level protein production in mammalian cells. *Acta Crystallogr. Sect. D Biol. Crystallogr.* **62**, 1243–1250.
56. O'Callaghan, C.A., Byford, M.F., Wyer, J.R., Willcox, B.E., Jakobsen, B.K., McMichael, A.J., Bell, J.I., (1999). BirA enzyme: Production and application in the study of membrane receptor-ligand interactions by site-specific biotinylation. *Anal. Biochem.* **266**, 9–15.
57. Pardon, E., Laeremans, T., Triest, S., Rasmussen, S.G.F., Wohlkönig, A., Ruf, A., Muyldermans, S., Hol, W.G.J., Kobilka, B.K., Steyaert, J., (2014). A general protocol for the generation of Nanobodies for structural biology. *Nature Protoc.* **9**, 674–693.
58. Robert, X., Gouet, P., (2014). Deciphering key features in protein structures with the new ENDscript server. *Nucleic Acids Res.* **42**, W320–W324.
59. Hanke, L., Vidakovics Perez, L., Sheward, D.J., Das, H., Schulte, T., Moliner-Morro, A., Corcoran, M., Achour, A., Karlsson Hedestam, G.B., Hällberg, B.M., Murrell, B., McInerney, G.M., (2020). An alpaca nanobody neutralizes SARS-CoV-2 by blocking receptor interaction. *Nature Commun.* **11**, 4420.
60. Shi, J., Kundrat, L., Pishesha, N., Bilate, A., Theile, C., Maruyama, T., Dougan, S., Ploegh, H., Lodish, H., (2014). Engineered red blood cells as carriers for systemic delivery of a wide array of functional probes. *Proc. Natl. Acad. Sci. U S A* **111**, 10131–10136.
61. Chen, L., Cohen, J., Song, X., Zhao, A., Ye, Z., Feulner, C. J., Doonan, P., Somers, W., Lin, L., Chen, P.R., (2016). Improved variants of SrtA for site-specific conjugation on antibodies and proteins with high efficiency. *Sci. Rep.* **6**, 31899.
62. Fisher, L., Lindner, W., Young, M., Termine, J., (1989). Synthetic peptide antisera: their production and use in the cloning of matrix proteins. *Connect. Tissue Res.* **21**, 43–48.
63. Devillard, L., Vandroux, D., Tissier, C., Brochot, A., Voisin, S., Rochette, L., Athias, P., (2006). Tubulin ligands suggest a microtubule-NADPH oxidase relationship in postischemic cardiomyocytes. *Eur. J. Pharmacol.* **548**, 64–73.
64. Kabsch, W., (2010). XDS. *Acta Crystallogr. Sect. D Biol. Crystallogr.* **66**, 125–132.
65. Evans, P.R., Murshudov, G.N., (2013). How good are my data and what is the resolution? *Acta Crystallogr. Sect. D Biol. Crystallogr.* **69**, 1204–1214.
66. McCoy, A.J., Grosse-Kunstleve, R.W., Adams, P.D., Winn, M.D., Storoni, L.C., Read, R.J., (2007). Phaser crystallographic software. *J. Appl. Crystallogr.* **40**, 658–674.
67. Emsley, P., Cowtan, K., (2004). Coot: Model-building tools for molecular graphics. *Acta Crystallogr. Sect. D Biol. Crystallogr.* **60**, 2126–2132.